Probing the Promiscuous Active Site of *myo*-Inositol Dehydrogenase Using Synthetic Substrates, Homology Modeling, and Active Site Modification†

Richard Daniellou,‡ Hongyan Zheng, David M. Langill, David A. R. Sanders, and David R. J. Palmer*

Department of Chemistry, University of Saskatchewan, 110 Science Place, Saskatoon, Saskatchewan, Canada S7N 5C9

Received February 9, 2007; Revised Manuscript Received April 21, 2007

ABSTRACT: The active site of *myo*-inositol dehydrogenase (IDH, EC 1.1.1.18) from *Bacillus subtilis* recognizes a variety of mono- and disaccharides, as well as 1L-4-O-substituted inositol derivatives. It catalyzes the NAD^+-dependent oxidation of the axial alcohol of these substrates with comparable kinetic constants. We have found that 4-*O*-*p*-toluenesulfonyl-*myo*-inositol does not act as a substrate for IDH, in contrast to structurally similar compounds such as those bearing substituted benzyl substituents in the same position. X-ray crystallographic analysis of 4-*O*-*p*-toluenesulfonyl-*myo*-inositol and 4-*O*-(2-naphthyl)-methyl-*myo*-inositol, which is a substrate for IDH, shows a distinct difference in the preferred conformation of the aryl substituent. Conformational analysis of known substrates of IDH suggests that this conformational difference may account for the difference in reactivity of 4-*O*-*p*-toluenesulfonyl-*myo*-inositol in the presence of IDH. A sequence alignment of IDH with the homologous glucose−fructose oxidoreductase allowed the construction of an homology model of inositol dehydrogenase, to which NADH and 4-*O*-benzyl-*scyllo*-inosose were docked and the active site energy minimized. The active site model is consistent with all experimental results and suggests that a conserved tyrosine−glycine−tyrosine motif forms the hydrophobic pocket adjoining the site of inositol recognition. Y233F and Y235F retain activity, while Y233R and Y235R do not. A histidine−aspartate pair, H176 and D172, are proposed to act as a dyad in which H176 is the active site acid/base. The enzyme is inactivated by diethyl pyrocarbonate, and the mutants H176A and D172N show a marked loss of activity. Kinetic isotope effect experiments with D172N indicate that chemistry is rate-determining for this mutant.

Inositol dehydrogenase (EC 1.1.1.18) from *Bacillus subtilis* (IDH)[1] is an NAD^+-dependent enzyme that catalyzes the regioselective oxidation of the axial hydroxyl group of *myo*-inositol to form *scyllo*-inosose, as shown in Scheme 1 (*1*). The gene encoding IDH is found in the *iol* operon for *myo*-inositol catabolism, which allows *B. subtilis* to grow on inositol as the sole carbon source (like many environmental bacteria) (*2*). IDH is known to be promiscuous with respect to substrate recognition; it will oxidize α-D-glucose, and recently we observed (*3*) that IDH could also oxidize certain α-(1,6)-linked disaccharides and inositols bearing a 4-*O*-alkyl or acyl substituent. This latter class of artificial substrates is oxidized stereoselectively; only the 1L-4-O-substituted *myo*-inositols are oxidized, while the 1D-enantiomer is neither substrate nor inhibitor. Perhaps most surprising is the size of substituent accommodated, the largest observed being the (10*S*)-camphorsulfonyl group. Compounds like 1L-4-*O*-benzyl-*myo*-inositol (**1**) have an apparent K_m that is lower than that of *myo*-inositol itself. A charged substituent, such as the *p*-carboxybenzyl or phosphoryl group, results in lowered activity. These observations suggest that IDH contains a hydrophobic pocket at its active site that can accommodate these large, neutral substituents. Previous work (*1*) has shown that other monosaccharides, such as D-mannose, D-galactose, and 2-deoxy-D-glucose, are not substrates, but D-xylose is oxidized with comparable efficiency to D-glucose. These observations can be rationalized by invoking active site recognition of equatorial hydroxyl groups in the 2-, 3-, and 4-positions of a D-pyranose ring. Recently, *chiro*-inositol was reported to be a substrate for IDH (*4*), suggesting a less stringent requirement in this position, consistent with the active site's tolerance for pyranoses.

Scheme 1: Reactions Catalyzed by IDH

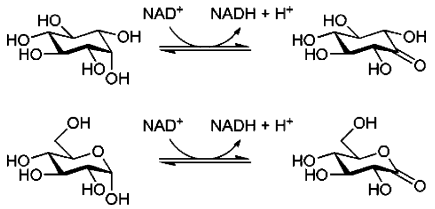

† This work was supported by a Discovery Grant from the Natural Sciences and Engineering Research Council of Canada (NSERC). The authors thank the Saskatchewan Health Research Foundation for funding the Molecular Design Research Group of the University of Saskatchewan.

* To whom correspondence should be addressed: telephone, (306) 966-4662; fax, (306) 966-4730; e-mail, palmer@sask.usask.ca.

‡ Present address: UMR CNRS 6226, Ecole Nationale Supérieure de Chimie de Rennes, Avenue du Général Leclerc, 35700 Rennes, France.

[1] Abbreviations: DEPC, diethyl pyrocarbonate; DMSO, dimethyl sulfoxide; ESMS, electrospray mass spectrometry; GFOR, glucose−fructose oxidoreductase; HPLC, high-performance liquid chromatography; IDH, inositol dehydrogenase; NAD^+, nicotinamide adenine 5′-dinucleotide (oxidized form); NADH, nicotinamide adenine 5′-dinucleotide (reduced form); $NADP^+$, nicotinamide adenine 5′-dinucleotide 3′-monophosphate (oxidized form); NADPH, nicotinamide adenine 5′-dinucleotide 3′-monophosphate (reduced form); rmsd, root mean square deviation.

10.1021/bi700281x CCC: $37.00
Published on Web 06/01/2007

IDH is a member of a group of homologous dehydrogenases that is well represented in bacteria but for which there is limited structure−function relationship information available. Some of these homologues, such as those called "MocA", are apparently inositol dehydrogenases, while many open reading frames identified by sequencing projects encode proteins known only as "putative oxidoreductases". There is no crystallographic information available for IDH, but there is a structure available for an IDH homologue, glucose−fructose oxidoreductase (GFOR), complexed with NADPH (*5*, *6*). The structure of GFOR can be used as a template to build an homology model of IDH, but information regarding the conformation of the substrate would strengthen any conclusions regarding the active site structure. Here we report a more complete exploration of the active site using synthetic substrates and a conformational analysis of those compounds. Sequence alignment and homology modeling allowed prediction of several active site residues responsible for binding and/or catalysis. We have tested these predictions using affinity labeling and site-directed mutagenesis.

MATERIALS AND METHODS

Chemical reagents, including buffers, salts, *myo*-inositol, NAD^+, and NADH, were obtained from Sigma-Aldrich Canada, Ltd. (Oakville, Ontario, Canada), or VWR CanLab (Mississauga, Ontario, Canada) and were categorized as molecular biology grade or were of the highest grade available. *scyllo*-Inosose was synthesized as previously described, and its spectroscopic characteristics matched those reported before (*7*). Inositol dehydrogenase was purified as we described elsewhere (*3*, *8*). UV−visible absorbance was measured using a Beckman DU-640 spectrophotometer with a circulating-bath-controlled temperature block. NMR spectra were recorded on a Bruker 500 MHz spectrometer. Chemical shifts are reported in parts per million downfield from tetramethylsilane (external standard). Electrospray mass spectra of inositol derivatives were recorded using a VG 70SE mass spectrometer. HPLC-ESMS was performed on a fee-for-service basis at the Saskatoon Cancer Centre. Thin-layer chromatography was performed on aluminum-backed plates of silica gel $60F_{254}$ (EM Science, Gibbstown, NJ) using phosphomolybdic acid/ethanol reagent, or a 10% solution of sulfuric acid in ethanol, and/or UV at 254 nm to visualize spots. Silica gel 60 (40−63 μm) was used for flash chromatography.

Organic Synthesis. Synthesis of 4/6-O-substituted *myo*-inositol derivatives followed the general procedure reported previously (*3*, *8*), with minor modifications. Details for each novel compound are given in the Supporting Information. Synthesis of *myo*-[2-^{2}H]inositol was described previously (*9*), and isotope effects were measured relative to (nondeuterated) *myo*-inositol synthesized by the same procedure. All substrates were homogeneous by ^{1}H NMR spectroscopy. Novel compounds were characterized by high-resolution mass spectrometry and/or elemental analysis.

Enzyme Kinetics. Compounds were screened as substrates at concentrations of 100 mM. Assays were performed and kinetic constants determined as described previously (*3*), fitting the data to the Michaelis−Menten equation:

$$v = V^{app}[S]/(K^{app} + [S])$$

Cosolvents were tested using buffer solutions mixed volume/volume with the cosolvent of interest, which were then made 20 mM in inositol. Kinetic constants for the mutant enzymes were calculated by varying both substrates, as described previously (*9*), fitting the data to the equation for an ordered sequential Bi-Bi mechanism in the absence of products:

$$v = \frac{V_{max}[A][B]}{K_{iA}K_{mB} + K_{mB}[A] + K_{mA}[B] + [A][B]}$$

Molecular Modeling of the Substrates. All calculations were performed using the software SPARTAN'04 for PC (Wavefunction). The molecules were built using the crystal structure of 4-*O*-*p*-toluenesulfonyl-*myo*-inositol or 4-*O*-(2-naphthyl)methyl-*myo*-inositol (*10*) as the starting point and then energy minimized using the PM3 semiempirical force field. A conformational search using SPARTAN'04 was used to ascertain the lowest energy conformation. Molecular dynamics simulations at 1000 K, followed by energy minimization of conformers along the runs, were performed using the Discover module of InsightII software to support the findings.

Sequence Analysis. Amino acid sequences were aligned using ESPript (*11*) or using CLUSTALW 1.83 (*12*), with the BLOSUM 62 scoring matrix (gap penalty = 10, gap extension penalty = 0.5).

Homology Modeling of IDH and Docking of the Substrates. The search for sequences similar to IDH (accession no. AAT78431) within the Protein Data Bank (PDB) (*13*) was performed with the BLAST program (*14*). The coordinates of the crystal structure of one monomer of GFOR from *Zymomonas mobilis* (Brookhaven Protein Data Bank access entry code 1OFG) was used as the template to build the model. Sequence alignment was performed using T-Coffee (*15*) and then manually adjusted. The 3D model of IDH was generated using the software MODELLER 8.2 (*16*) with default parameters. Hydrogen atoms were added to the protein at standard positions, and the entire resulting structure obtained was optimized by energy minimization using the Discover module of InsightII (Accelrys, Inc.) with the default force field parameters. Subsequently, NADH was docked by constraint, based on the binding of NADH observed in the truncated GFOR from *Z. mobilis* (Brookhaven Protein Data Bank access entry code 1EVJ). Finally, the substrate 1L-4-*O*-benzyl-*scyllo*-inosose was manually docked into the active site, and the energy of the ternary complex active site residues and ligands was minimized using InsightII. The overall quality of the model was confirmed using PROCHECK (*17*) and compared to its template. Structural alignment with GFOR was performed using DALIlite (*18*).

Inactivation of IDH with Diethyl Pyrocarbonate (DEPC). The DEPC reagent was freshly diluted with cold ethanol for each experiment. Carbethoxylation was carried out by incubating 0.24 mg of IDH with an appropriately diluted reagent in 0.1 M potassium phosphate buffer, pH = 7.1. The final concentration of ethanol in the reaction mixture never exceeded 2% by volume and was found to have no effect on the activity nor stability of the enzyme during the incubation time. The extent of inactivation was determined

by measuring the residual enzyme activity at 25 °C using the following conditions: 5 mM *scyllo*-inosose, 0.1 mM NADH, and 1.2 μg of inactivated enzyme in 0.1 M potassium phosphate buffer, pH = 7.1, and 25 °C. In the protection experiments, the enzyme was preincubated with the substrate for 1 min prior to addition of DEPC to a concentration of 0.2 mM.

Chymotryptic Digestion and HPLC−Electrospray Ionization Mass Spectrometry. Aliquots of 100 μL of DEPC-modified IDH and unmodified IDH were purified by ultrafiltration using a Centricon microconcentrator 10000. Retentates were washed three times with 100 μL of 50 mM potassium phosphate buffer, pH 7.0. All retentates were collected and were dissolved in 100 μL of 6 M guanidine hydrochloride and 2 mM β-mercaptoethanol solution in 50 mM potassium phosphate buffer, pH 7.0. The resulting solutions were placed in a 37 °C water bath for 1 h and then purified and washed again by ultrafiltration. Retentates were finally dissolved in 80 μL of 50 mM potassium phosphate buffer, pH 7.0. The samples were incubated at 37 °C with 0.5 μL of a 5 mg/mL solution of α-chymotrypsin, with an additional 0.25 μL added after the first and second hour to a total of 5 μg of digesting enzyme. The total time for enzyme digestion was 4 h. Protein digests were analyzed using a Waters 2796 Bioseparations module coupled to a Waters 2487 dual absorbance detector. The separation used a Waters Biosuite C18 PA-A 3 μm, 2.1 × 250 mm column with a flow rate of 0.2 mL/min. The initial conditions consisted of water/formic acid (99.9/0.1) and were held for 5 min followed by a linear gradient to water/acetonitrile/formic acid (40/60/0.1) in 60 min. The absorbance at λ = 220 nm was monitored on-line prior to MS. The HPLC effluent was directed to a Micromass LCT mass spectrometer. Positive ion mass spectra were acquired in the *m*/*z* range of 400−2000. Peptide fragments of the chymotryptic digest were predicted using the computer program PeptideMass (http://www.expasy.org/tools/peptide-mass.html). A table of predicted fragments is included in the Supporting Information. A fragment of molecular weight 824.5 was predicted to contain His-176. To identify the chromatographic peak of interest, the eluent was examined initially in 10 min fractions; then the fraction between 20 and 30 min was examined peak by peak until the one containing a mass of 824.5 was found.

Site-Directed Mutagenesis. The mutants of IDH were generated using the QuikChange site-directed mutagenesis kit from Stratagene (La Jolla, CA) according to manufacturer's directions, except that an extension time of 2 min per kilobase gave better results than the recommended 1 min per kilobase. The template plasmid was pET-28b into which the IDH gene had been subcloned, as previously described (*3*). For each mutant, a set of mutagenic primers were designed to incorporate a change in the nucleotide sequence coding for the residue of interest. In the case of H176A and D172N, the altered sequence resulted in the deletion of a restriction site, and this was exploited to screen transformants for positive mutations. For other mutants, an additional, silent mutation was introduced to generate a new restriction site for the purpose of screening. A complete list of primer sequences is included in the Supporting Information.

After screening transformants, selected clones were tested for expression by transformation into *Escherichia coli* BL21-(DE3). All selected clones showed expression similar to that of the wild-type enzyme. A clone was selected, and the complete open reading frame was sequenced (National Research Council Plant Biotechnology Institute DNA Technologies Unit, Saskatoon, Saskatchewan, Canada) in order to ensure no other mutations had been introduced. The protein was purified as previously described for the wild-type enzyme but using columns which had never been in contact with wild-type IDH.

RESULTS AND DISCUSSION

Natural and Synthetic Candidate Substrates. Chart 1 shows the array of natural and synthetic inositols and sugars discussed below. The systematic numbering for inositol derivatives is also indicated. (The isomers shown could be named as the 1D-6-O-substituted or the 1L-4-O-substituted inositols. By rule, the descriptor should be the lowest number possible; therefore, we have used the 1L numbering.) For clarity, we have also shown the systematic numbering of the D-sugars. Ramaley et al. (*1*) reported that α-D-glucose and D-xylose were alternative substrates for IDH but that D-mannose and D-galactose were not; D-ribose and D-fructose showed "trace activity". We have confirmed these findings, although we observe no activity on ribose and fructose, and we suspect the "trace" may be due to the presence of contamination by D-glucose. A systematic approach demands that D-allose, containing an axial hydroxyl group at carbon 3, also be tested. In our hands, this compound is not a substrate, confirming the preference of the enzyme for equatorial substituents in the 2-, 3- and 4-positions of monosaccharides (corresponding to the L1-, 6-, and 5-positions of *myo*-inositol, as indicated in Chart 1). We have confirmed the report that *chiro*-inositol is a substrate (*4*), with an approximately 2-fold greater apparent K_m (37 ± 4 mM), indicating that there is a minor discrimination at position 1L-3, corresponding to the position occupied by oxygen in the D-pyranose series.

The synthesis of racemic inositol derivatives functionalized selectively at the 4/6-position was achieved using the orthoformate-protection route introduced by Kishi (*19*), as we have described previously (*3*, *8*). Virtually any activated electrophile may be used to substitute the inositol ring, with the limitation that these substrate candidates need to be water-soluble. In order to overcome this limitation, cosolvents were tested using the natural substrate *myo*-inositol. Adding 10% (v/v) dioxane, acetonitrile, or dimethylformamide resulted in a dramatic loss of activity. However, more than 80% activity can be retained in up to 15% methanol, as well as up to 40% dimethyl sulfoxide (DMSO). The enzyme is fully active in 20% DMSO. We had already demonstrated the presence of a hydrophobic pocket that could accommodate sugar residues, suggesting to us that the pocket had some aromatic character. Now we can see that substituents as long as the *trans*-cinnamyl and (2-naphthyl)methyl groups will fit in this pocket, as shown in Table 1. Using the *o*-, *m*-, and *p*-methylbenzyl substituents (**7**−**9**), a preference for the para-substituted **9** suggests a steric interaction that disfavors bulkier or branching substituents. This is also consistent with the greater K_m value observed for the glucosyl inositol **13**. Surprisingly, the 4-*O*-*p*-toluenesulfonyl derivative **12** was not recognized by the enzyme, despite steric and electronic

Chart 1

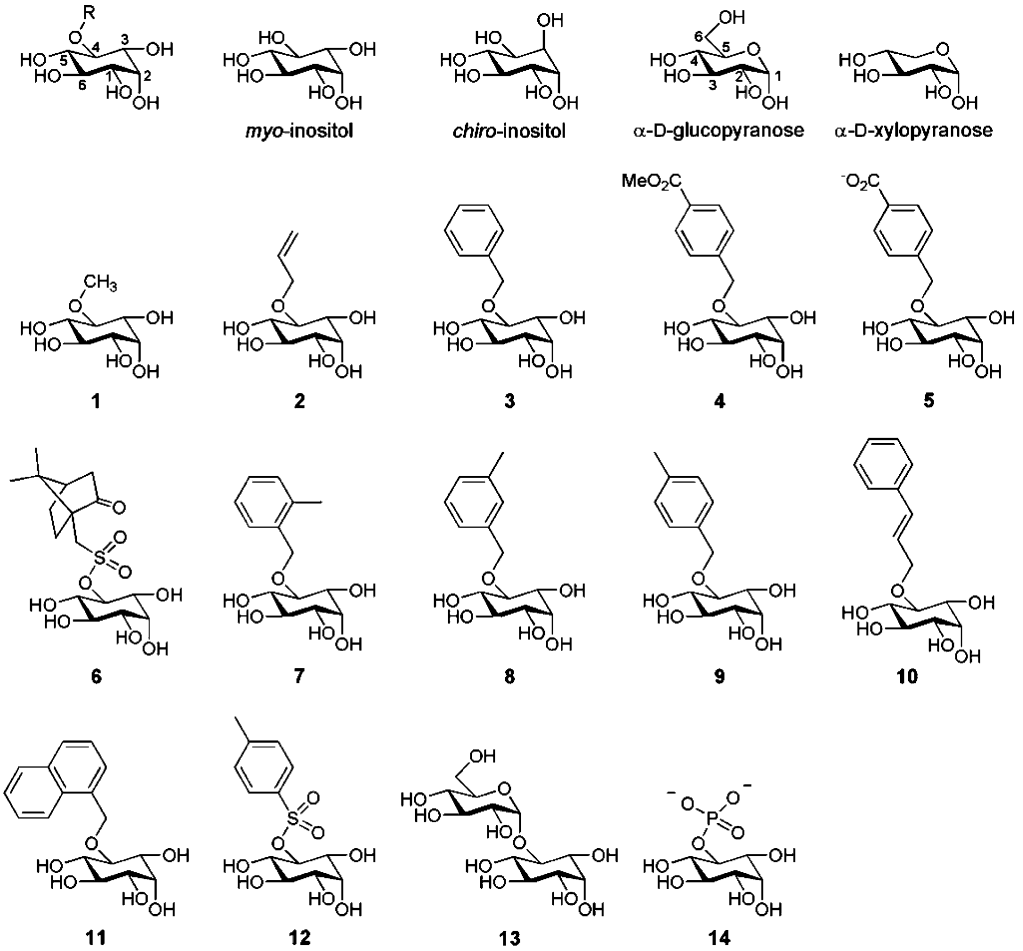

Table 1: Kinetic Constants of IDH-Catalyzed Oxidations[a]

compound	R	K^{app}/mM	V^{app}/μmol min^{-1} mg^{-1}
myo-inositol[b]	H	18 ± 2	8 ± 1
1[b]	Me	8 ± 1	0.8 ± 0.1
2[b]	allyl	7 ± 1	0.8 ± 0.1
3[b]	benzyl	4 ± 1	0.9 ± 0.1
4[b]	*p*-(methyloxycarbonyl)-benzyl	3 ± 1	0.8 ± 0.1
5[b]	*p*-carboxybenzyl	44 ± 5	1.6 ± 0.1
6[b]	(1*S*)-10-camphor-sulfonyl	13 ± 2	0.7 ± 0.1
7	*o*-methylbenzyl	9.5 ± 1	0.7 ± 0.1
8	*m*-methylbenzyl	8.5 ± 1	0.7 ± 0.1
9	*p*-methylbenzyl	3 ± 1	0.7 ± 0.1
10	*trans*-cinnamyl	13 ± 1	3 ± 0.1
11[c]	(2-naphthyl)methyl	18 ± 3	0.9 ± 0.1
12	*p*-toluenesulfonyl		
13[d]	α-D-glucopyranosyl	18 ± 2	4.0 ± 0.5
14[b]	phosphate	trace activity	

[a] Conditions: 100 mM Tris-HCl, pH 9.0, 25 °C. [NAD^+] = 0.5 mM. Where R is listed, refer to Chart 1. [b] Data from ref *2*. [c] Conditions: 100 mM Tris-HCl containing 20% DMSO, pH 9.0, 25 °C. [NAD^+] = 0.5 mM. [d] Data from ref *8*.

characteristics similar to many of the compounds that are substrates.

Conformational Analysis of Substrates. Compounds **11** and **12** have been crystallized and high-resolution X-ray structures determined (*10*). These compounds adopt strikingly dissimilar conformations (Figure 1); the plane of the naphthyl substituent of **11** is tilted only about 18° to the inositol chair, whereas in **12** the aromatic ring is at a nearly orthogonal angle of about 81° to the chair. The coordinates of these two conformations were used as starting points for conformational analyses using semiempirical calculations and molecular dynamics simulations, which confirmed that the structures represented the minimum energy conformations. Other aromatic substrates from Table 1 were also tested by the same methods, using the structures of **11** and **12** as starting points. In all cases, the aromatic substituent preferred a conformation similar to that of **11**, consistent with this conformational preference being a requirement for binding to the active site of IDH. Figure 1 shows the altered orientation of the substituent of **12** relative to those acting as substrates. The incompatibility of the preferred conformation of **12** for the active site may be due to steric effects, unfavorable electronic (e.g., dipole−dipole) interactions, or both.

Homology Modeling of IDH. In the absence of high-resolution structural data, the primary sequence can be compared to those of other, better characterized proteins in order to gain an understanding of the features of the protein and their role in catalysis. Unfortunately, few members of this subfamily of dehydrogenases have been characterized to a sufficient extent to allow such comparisons. There have been no structural studies of IDH beyond the determination that the enzyme exists as a tetramer, and in our hands diffraction-quality crystals have not been attained. IDH is a member of a group of homologous oxidoreductase enzymes that includes glucose−fructose oxidoreductase (GFOR),

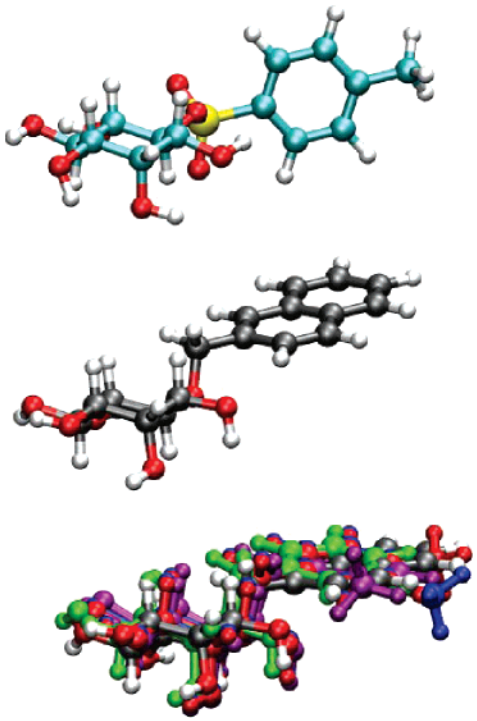

FIGURE 1: Top: CPK model built from the crystal structure of **12** (carbon, cyan; oxygen, red; sulfur, yellow; hydrogen, white). Middle: CPK model built from the crystal structure of **11** (carbon, black; oxygen, red; hydrogen, white). Bottom: Superposition of the structure of **11** with the energy-minimized structures of **3** (green), **7** (magenta), **8** (blue), and **9** (red). Images generated using VMD (Urbana, IL), followed by POV-Ray 3.6 (Victoria, Australia).

galactose dehydrogenase, biliverdin reductase, and several other sequences, most of whose specific functions are not yet well established (*20*). Of these, GFOR has been crystallized, and the high-resolution structures of the wild-type enzyme and several mutants have been determined by X-ray crystallography (*21*). From the structure of GFOR, sequence alignments allow predictions regarding the roles of residues found in IDH, limited by the differences between the two reactions catalyzed: GFOR catalyzes the $NADP^+$-dependent oxidation of D-glucose to gluconolactone (like the IDH reaction of Scheme 1) but also the reduction of fructose to sorbitol without release of the tightly bound cofactor. GFOR has not been crystallized in the presence of a sugar substrate but with succinate and glycerol bound at the active site. This gives only minimal information regarding the substrate-binding pocket, but the authors suggested that Arg-252, Asp-265, and Tyr-269 may participate in the recognition and/or activation of the substrate; Tyr-269 and Asp-265 were proposed as a catalytic dyad, with the tyrosine residue proposed to abstract the proton from the hydroxyl group in the reaction. Because of the presence of NADPH in the structures, GFOR residues implicated in the binding of this molecule are known with much greater certainty, specifically Tyr-94, Gly-95, Ser-116, Glu-180, Lys-181, Trp-251, and Arg-252. The sequence alignment in Figure 2 predicts that the residues in IDH involved in binding NADH are Ile-13, Gly-14, Asp-35, Glu-96, Lys-97, Asp-162, and Asn-163. Notably, the serine residue at position 116 of GFOR is replaced by an aspartate residue at position 36 of IDH. This is expected. NADH-dependent enzymes like IDH typically have an aspartate residue in this position, interacting with the 2′-hydroxyl group of the adenosine ribose (*22*). NADPH-dependent enzymes must recognize a phosphate group at this position, which they do using a Ser residue (*20*, *22*, *23*). We were most interested in the sugar-binding site, and sequence alignments suggested that the Tyr-Asp dyad in GFOR was present in IDH as a His-Asp dyad, specifically His-176 and Asp-172. Arg-252 of GFOR is found in a region bearing no resemblance to the sequence of IDH. Therefore, no firm clues could be found regarding the recognition of inositol substrates nor the proposed hydrophobic pocket adjoining the active site.

GFOR and IDH share only 18% sequence identity overall, but it is now well-established that homologous enzymes, even those with relatively low sequence identity, will have a conserved protein fold, with considerable conservation of active site architecture (*24*−*26*). We therefore constructed an homology model, as described in Materials and Methods, with the understanding that the results based on such low overall sequence identity might be prone to error in detail, and any predictions based on this model would have to be fully corroborated by experimental evidence. The generated model was energy minimized using the Discover module of InsightII (Accelrys), and the substrates NADH and 1L-4-*O*-benzyl-*myo*-inosose were docked manually, and the energy of the active site reminimized. The resulting model, shown in Figure 3, was judged to be valid using the PROCHECK program, indicating that 87% of the residues were in the most favored regions and 12% in additionally allowed regions. This result is superior to the GFOR structure on which the model was based. A Ramachandran plot is included in the Supporting Information. Structural alignment indicated an rmsd of 2.2 Å.

Active Site Residue Prediction. Docking of NADH to the IDH model could be done with reasonable confidence, knowing its position in the crystal structure of GFOR and in other proteins containing the so-called Rossmann fold. This docking positions carbon 4 of the nicotinamide moiety 5.9 Å from His-176, the proposed active site acid/base catalyst. Substrate inosose was docked so that a hydride could be delivered to the carbonyl carbon from the nicotinamide to result in an axial hydroxyl group. This resulted in a distance from the Nϵ atom of His-176 to the carbonyl oxygen of about 3 Å, as shown in Figure 3. A highly conserved GFMRR motif of residues starting at position 124 of the IDH sequence defines one side of the active site and may be responsible for the recognition of equatorial hydroxyl groups discussed above. Position L3 of the substrate, which can bear either an axial or equatorial substituent, shows no apparent contact with surrounding protein residues and appears to be solvent-accessible.

The hydrophobic cavity associated with the recognition of large substituents at position L4 is evident in the model. The cavity is delimited by several residues: His-155, Tyr-233, Gly-234, Tyr-235, Pro-253, and Gln-341. Of these, the YGY motif at positions 233−235 seems to form an aromatic sandwich between which the substituent can insert. This YGY motif is highly conserved among IDH sequences (see Supporting Information). The precise role of this cavity with respect to metabolic function of IDH is not clear, but its conservation suggests that this motif plays some important catalytic or structural role. A striking feature of the model is that the position of this apparent cavity is completely consistent with the stereoselectivity displayed by the enzyme;

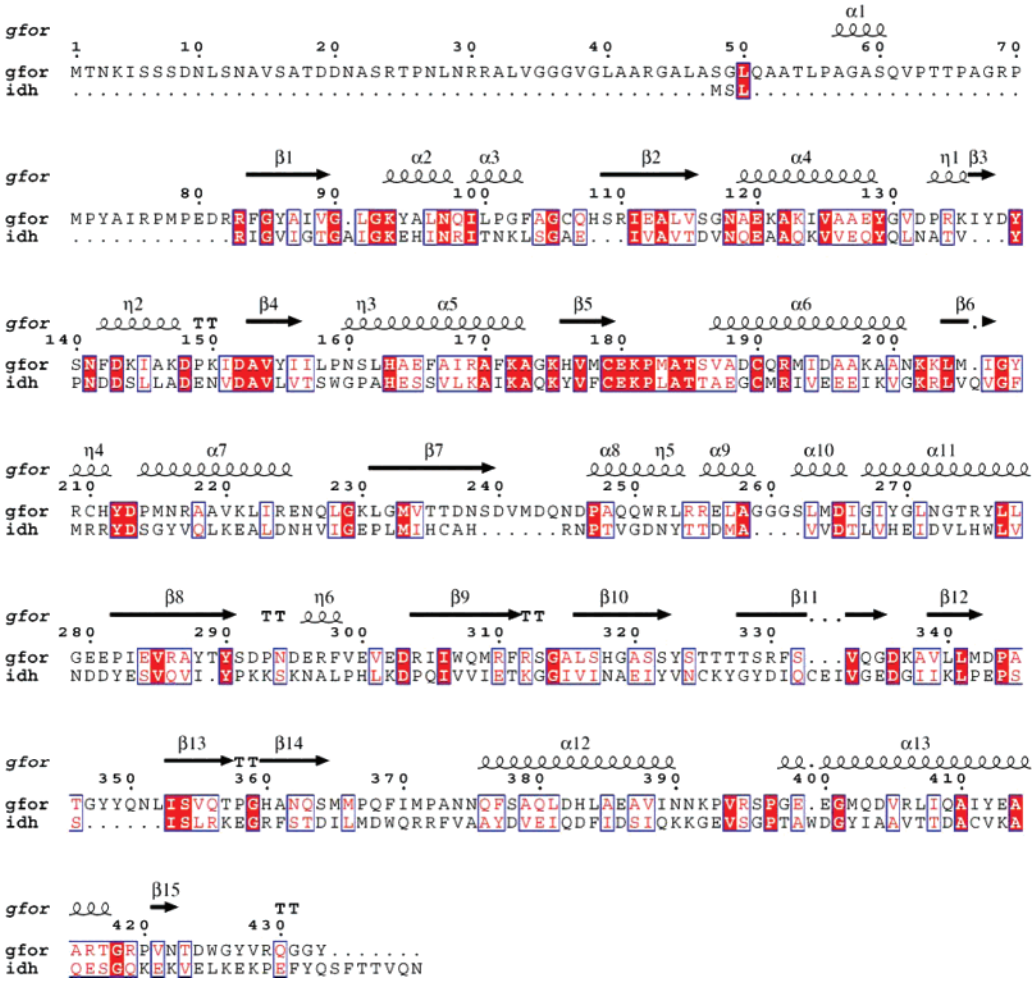

FIGURE 2: Sequence alignment, generated using ESPript, of GFOR with IDH used to construct the homology model.

that is, a 1D-4-O-substituted inositol would not bind productively to the active site.

DEPC Modification. Sequence alignment and homology modeling support the proposal that His-176 is the active site acid/base catalyst. DEPC reacts selectively with accessible histidine residues to form *N*-carbethoxyhistidine in a pH range of 5.5−8.0 (*27*). During our experiments, no tyrosine residues were apparently modified using DEPC, as monitored at 278 nm. Reaction with DEPC resulted in a loss of enzyme activity dependent on time and DEPC concentration. Monitoring the solution at 240 nm (*28*) indicated that 0.6 mM DEPC reacted with all 14 histidine residues of the protein in 15 min. Preincubation with 1 mM NADH resulted in protection of 80% of the IDH activity. Treatment of the inactivated enzyme with 20 mM hydroxylamine for 48 h at room temperature resulted in a complete recovery of the native activity, showing that the action of the reagent is reversible and that the residue modified is most likely a histidine.

α-*Chymotryptic Digestion and HPLC-MS*. The site of DEPC modification can be determined by mass spectrometry of the peptide fragments of a digested sample of inactivated enzyme (*29*). Three different samples were digested and analyzed by HPLC-MS: first, the native protein; second, a DEPC-inactivated IDH; and third, a similarly treated sample protected by the substrate NADH. Digestion with α-chymotrypsin resulted in peptide fragments; the fragment containing His-176 is predicted to have a mass of 824.5 (Val-175 to Leu-181). All samples were digested at pH 7.0 for 4 h at 37 °C and showed similar HPLC chromatograms. The peptide of interest was found to have, in our conditions, a retention time of 26.5 min. This peptide could be identified in the native and substrate-protected IDH samples but was absent from the DEPC-modified sample (see Supporting Information), suggesting that the mass and/or retention time of this fragment had been altered. Together with the results described above, we conclude that His-176 is present at the active site and required for catalysis.

Site-Directed Mutagenesis. On the basis of sequence alignment and modeling, we felt that five residues in particular stood out as candidates for mutagenesis. His-176 is the proposed active site acid/base catalyst, and this was supported by the DEPC experiments. We predicted that mutation of this histidine to alanine would have a very large effect on catalysis. It is reasonable to expect some residual activity in such a mutant, since deprotonation is not the primary driving force of the hydride transfer reaction. Asp-172 is the second member of the proposed catalytic dyad discussed above, and mutation of this residue to isosteric asparagine is expected to modify the reactivity to a lesser extent than mutation of His-176. Asp-179 is also a conserved residue among IDH sequences, but not in GFOR, and the homology model suggests it is likely too far from His-176 to participate in a canonical catalytic dyad. Nevertheless, we felt that there was sufficient evidence to consider this residue a candidate for a catalytic role in the reaction. Our model

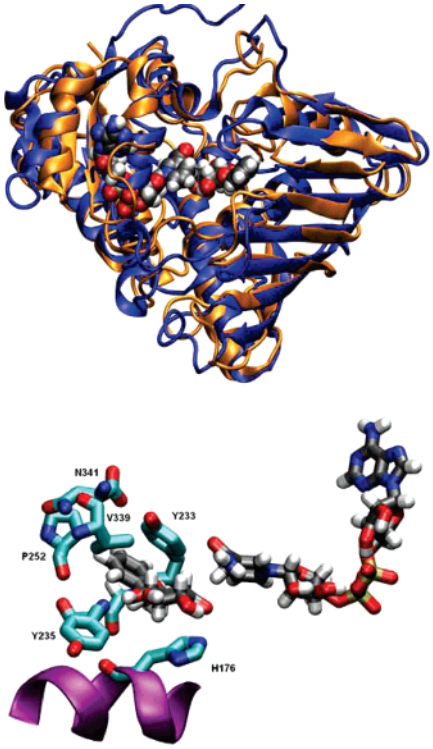

FIGURE 3: Top: Ribbon diagram of the structural alignment of the crystal structure of GFOR (blue) and the homology model of IDH (orange) with the substrates NADH and inosose bound in the active site. Bottom: Active site model of IDH (protein carbon atoms are shown in cyan; substrate carbon atoms are shown in black; oxygen atoms, red; nitrogen atoms, blue; hydrogen atoms, white; phosphorus atoms, gold). Images generated using VMD (Urbana, IL), followed by POV-Ray 3.6 (Victoria, Australia).

shows Tyr-233 and Tyr-235 form an aromatic pocket, but they may also play some role in the structural integrity of the active site. Mutation of these residues may alter the activity, or the substrate spectrum, or both. Indeed, the model indicates that the hydroxyl group of Tyr-235 is 3.2 Å from the backbone amide carbonyl group of His-176 and near other residues on the α-helix that contains His-176 (see Figure 3). We chose therefore to construct conservative mutants Y233F and Y235F and nonconservative mutants Y233R and Y235R. The latter mutations were chosen in order to create a positively charged site that would tolerate, for example, a phosphate group as in **14**.

The results of the mutagenesis experiments are shown in Table 2. H176A showed a strikingly decreased turnover number, accompanied by an increased K_m for *myo*-inositol. The K_m for NAD^+ shows a relatively small change. The specificity constant for *myo*-inositol is 4 orders of magnitude lower than that of wild-type IDH, consistent with the disruption of a key catalytic residue.

Mutation of Asp-172 to asparagine resulted in a mutant that was impaired with respect to catalysis, but considerably less so than H176A. Indeed, the turnover number for D172N is considerably lower, and K_m for both inositol and NAD^+ have increased moderately, as would be predicted for the secondary partner in the catalytic dyad. The increase in the Michaelis constant for NAD^+ is consistent with the homology model, which places this residue in proximity to the endocyclic nitrogen of the nicotinamide ring.

We have previously reported (*9*) that no primary kinetic isotope effect was observed for wild-type IDH using [2-^{2}H]-*myo*-inositol. This result was consistent with the fact that product release is rate-determining. Using D172N, the oxidation of [2-^{2}H]-*myo*-inositol was now measurably slower: $k_{cat} = 0.6 \pm 0.1\ s^{-1}$, $K_m(NAD^+) = 1.5 \pm 0.6$ mM, and K_m([2-^{2}H]inositol) $= 39 \pm 17$ mM. The measured kinetic isotope effects were therefore 3.1 ± 0.4 on k_{cat} and 1.8 ± 0.9 on k_{cat}/K_m(inositol). This clearly indicates that the chemical step, hydride transfer to NAD^+, is now rate-determining.

Mutation of Asp-179 to asparagine resulted in much smaller effects on the reaction kinetics than the corresponding change to Asp-172. The mutant D179N shows decreased affinity for both substrates, but a small increase in turnover, such that the apparent second-order rate constant with respect to inositol is only 5-fold lower than that of wild-type IDH. This result is not consistent with Asp-179 participating in a catalytic dyad with His-176. Product release is the rate-determining step for the IDH-catalyzed reaction, and the small increase in turnover may result from the decreased substrate/product affinity.

The tyrosine residues predicted to form a hydrophobic pocket adjoining the active site were mutated to phenylalanine residues in order to test the importance of the hydroxyl group to catalysis for each residue. Catalysis by Y233F was decreased very little from the wild-type enzyme (Table 2), but Y235F was markedly impaired, suggesting that the hydroxyl group does play an important role. The largest effect was on the measured Michaelis constant for inositol. The hydroxyl group of Tyr-235 may keep this residue oriented appropriately or may interact directly with His-176. Conservation of the tyrosine may serve to position other groups in the active site in order to accommodate inositol in a position ideal for reaction. The nonconservative mutants Y233R and Y235R both showed no detectable activity toward inositol nor toward **14**.

During the preparation of this report, the crystal structure of 1,5-anhydro-D-fructose reductase was published (*30*). As was the case for GFOR, the structure is liganded with NADPH but not a sugar substrate. No aspect of that report contradicts our conclusions regarding IDH. Indeed, our

Table 2: Kinetic Constants of Site-Directed Mutants[a,b]

enzyme	$K_m(NAD^+)$ (mM)	K_m(inositol) (mM)	k_{cat} (s^{-1})	k_{cat}/K_m(inositol) ($s^{-1}\,M^{-1}$)
wild type	0.08 ± 0.01	4.4 ± 0.5	58 ± 1	$(1.3 \pm 0.2) \times 10^4$
H176A	0.3 ± 0.1	118 ± 7	0.23 ± 0.02	2.0 ± 0.3
D172N	1.1 ± 0.1	65 ± 1	1.9 ± 0.1	29 ± 2
D179N	0.4 ± 0.1	28 ± 5	73 ± 2	$(2.6 \pm 0.6) \times 10^3$
Y233F	0.07 ± 0.01	4.0 ± 0.4	47 ± 1	$(1.2 \pm 0.2) \times 10^4$
Y235F	0.11 ± 0.01	39 ± 3	34 ± 1	870 ± 9

[a] Conditions: 100 mM Tris-HCl, pH 9.0, 25 °C. Enzyme concentration $= 0.4 \pm 0.1$ μg/mL except H176A, 8.0 μg/mL; D172N, 1.6 μg/mL; Y233R, 50 μg/mL; Y235R, 37 μg/mL. [b] No activity was detected for mutants Y233R nor Y235R.

findings complement this work, which also proposes an analogous His-Asp dyad involved in catalysis.

In conclusion, we have probed the active site of IDH using synthetic substrate analogues to demonstrate the approximate capacity of a hydrophobic pocket adjoining the active site. A conformational preference of the toluenesulfonate group of **12** may account for its lack of reactivity in the presence of IDH. Sequence alignments suggested several residues involved in substrate recognition and catalysis of hydride transfer from inositol to NAD^+, although most residues involved in binding of inositol are not obvious based on sequence alignment alone. Homology modeling suggested strong candidates for recognition of the inositol and sugar-based substrates; specifically, a GFMR motif recognizing the equatorial hydroxyl groups on one side of the inositol ring and a YGY motif forming a hydrophobic pocket on the other side of the substrate. On the basis of DEPC labeling and site-directed mutagenesis experiments, we propose that His-176 is the acid/base catalyst involved in proton transfer from the axial hydroxyl group of inositol and that Asp-172 likely participates in this reaction in a secondary manner, as in a catalytic dyad. Isosteric mutation of Asp-179 to asparagine has only a modest effect on catalysis. The hydroxyl group of Tyr-235 is apparently important in catalysis, much more so than that of Tyr-233. Mutation of either tyrosine residue of the YGY motif to arginine abolishes activity. The model is completely consistent with the experimental observations, particularly the promiscuous but stereoselective recognition of the substituted inositol substrates. This work provides us with a new model to use to examine the structure−function relationships of the large group of homologous dehydrogenases active in bacteria.

ACKNOWLEDGMENT

Technical services provided by Ken Thoms and the Saskatchewan Structural Sciences Centre and by Karen Molochuk of the Saskatoon Cancer Centre are acknowledged.

SUPPORTING INFORMATION AVAILABLE

Synthesis and characterization of synthetic substrates, oligonucleotide primers for PCR reactions, Ramachandran plot of the homology model of IDH, alignment of selected IDH sequences, mass spectra of IDH fragment 195−201, and a table of predicted peptides from the chymotryptic digest of IDH. This material is available free of charge via the Internet at http://pubs.acs.org.

REFERENCES

1. Ramaley, R., Fujita, Y., and Freese, E. (1979) Purification and properties of *Bacillus subtilis* inositol dehydrogenase, *J. Biol. Chem. 254*, 7684−7690.
2. Yoshida, K. I., Aoyama, D., Ishio, I., Shibayama, T., and Fujita, Y. (1997) Organization and transcription of the myo-inositol operon, iol, of *Bacillus subtilis*, *J. Bacteriol. 179*, 4591−4598.
3. Daniellou, R., Phenix, C. P., Tam, P. H., Laliberte, M. C., and Palmer, D. R. J. (2005) Stereoselective oxidation of protected inositol derivatives catalyzed by inositol dehydrogenase from *Bacillus subtilis*, *Org. Biomol. Chem. 3*, 401−403.
4. Yoshida, K., Yamaguchi, M., Morinaga, T., Ikeuchi, M., Kinehara, M., and Ashida, H. (2006) Genetic modification of *Bacillus subtilis* for production of D-chiro-inositol, an investigational drug candidate for treatment of type 2 diabetes and polycystic ovary syndrome, *Appl. Environ. Microbiol. 72*, 1310−1315.
5. Lott, J. S., Halbig, D., Baker, H. M., Hardman, M. J., Sprenger, G. A., and Baker, E. N. (2000) Crystal structure of a truncated mutant of glucose-fructose oxidoreductase shows that an N-terminal arm controls tetramer formation, *J. Mol. Biol. 304*, 575−584.
6. Kingston, R. L., Scopes, R. K., and Baker, E. N. (1996) The structure of glucose-fructose oxidoreductase from *Zymomonas mobilis*: an osmoprotective periplasmic enzyme containing non-dissociable NADP, *Structure 4*, 1413−1428.
7. Hansen, C. A., Dean, A. B., and Frost, J. W. (1999) Synthesis of 1,2,3,4-tetrahydroxybenzene from D-glucose: exploiting *myo*-inositol as a precursor to aromatic chemicals, *J. Am. Chem. Soc. 121*, 3799−3800.
8. Daniellou, R., and Palmer, D. R. J. (2006) Appel-Lee synthesis of glycosyl inositols, substrates for inositol dehydrogenase from *Bacillus subtilis*, *Carbohydr. Res. 341*, 2145−2150.
9. Daniellou, R., Zheng, H., and Palmer, D. R. J. (2006) Kinetics of the reaction catalyzed by inositol dehydrogenase from *Bacillus subtilis* and inhibition by fluorinated substrate analogs, *Can. J. Chem. 84*, 522−527.
10. Daniellou, R., Quail, J. W., and Palmer, D. R. J. (2006) 4/6-*O*-(*p*-Tolylsulfonyl)-*myo*-inositol, *Acta Crystallogr., Sect. E: Struct. Rep. Online 62*, o4880−o4881.
11. Gouet, P., Courcelle, E., Stuart, D. I., and Metoz, F. (1999) ESPript: analysis of multiple sequence alignments in PostScript, *Bioinformatics 15*, 305−308.
12. Thompson, J. D., Higgins, D. G., and Gibson, T. J. (1994) Clustal-W—Improving the sensitivity of progressive multiple sequence alignment through sequence weighting, position-specific gap penalties and weight matrix choice, *Nucleic Acids Res. 22*, 4673−4680.
13. Bernstein, F. C., Koetzle, T. F., Williams, G. J. B., Meyer, E. F., Brice, M. D., Rodgers, J. R., Kennard, O., Shimanouchi, T., and Tasumi, M. (1977) Protein Data Bank—Computer-based archival file for macromolecular structures, *Eur. J. Biochem. 80*, 319−324.
14. Altschul, S. F., Gish, W., Miller, W., Myers, E. W., and Lipman, D. J. (1990) Basic local alignment search tool, *J. Mol. Biol. 215*, 403−410.
15. Notredame, C., Higgins, D. G., and Heringa, J. (2000) T-Coffee: A novel method for fast and accurate multiple sequence alignment, *J. Mol. Biol. 302*, 205−217.
16. Sali, A., and Blundell, T. L. (1993) Comparative protein modeling by satisfaction of spatial restraints, *J. Mol. Biol. 234*, 779−815.
17. Laskowski, R. A., Macarthur, M. W., Moss, D. S., and Thornton, J. M. (1993) Procheck—A program to check the stereochemical quality of protein structures, *J. Appl. Crystallogr. 26*, 283−291.
18. Holm, L., and Park, J. (2000) DaliLite workbench for protein structure comparison, *Bioinformatics 16*, 566−567.
19. Lee, H. W., and Kishi, Y. (1985) Synthesis of mono- and unsymmetrical bis- orthoesters of *scyllo*-inositol, *J. Org. Chem. 50*, 4402−4404.
20. Wiegert, T., Sahm, H., and Sprenger, G. A. (1997) The substitution of a single amino acid residue (Ser-116 → Asp) alters NADP-containing glucose-fructose oxidoreductase of *Zymomonas mobilis* into a glucose dehydrogenase with dual coenzyme specificity, *J. Biol. Chem. 272*, 13126−13133.
21. Nurizzo, D., Halbig, D., Sprenger, G. A., and Baker, E. N. (2001) Crystal structures of the precursor form of glucose-fructose oxidoreductase from *Zymomonas mobilis* and its complexes with bound ligands, *Biochemistry 40*, 13857−13867.
22. Fan, F., Lorenzen, J. A., and Plapp, B. V. (1991) An aspartate residue in yeast alcohol dehydrogenase-I determines the specificity for coenzyme, *Biochemistry 30*, 6397−6401.
23. Scrutton, N. S., Berry, A., and Perham, R. N. (1990) Redesign of the coenzyme specificity of a dehydrogenase by protein engineering, *Nature 343*, 38−43.
24. Gerlt, J. A., and Raushel, F. M. (2003) Evolution of function in (beta/alpha)(8)-barrel enzymes, *Curr. Opin. Chem. Biol. 7*, 252−264.
25. Wise, E. L., and Rayment, I. (2004) Understanding the importance of protein structure to nature's routes for divergent evolution in TIM barrel enzymes, *Acc. Chem. Res. 37*, 149−158.
26. Bartlett, G. J., Borkakoti, N., and Thornton, J. M. (2003) Catalysing new reactions during evolution: Economy of residues and mechanism, *J. Mol. Biol. 331*, 829−860.
27. Miles, E. W. (1977) Modification of histidyl residues in proteins by diethylpyrocarbonate, *Methods Enzymol. 47*, 431−442.

28. Olano, J., Soler, J., Busto, F., and de Arriaga, D. (1999) Chemical modification of NADP-isocitrate dehydrogenase from *Cephalosporium acremonium*—Evidence of essential histidine and lysine groups at the active site, *Eur. J. Biochem. 261*, 640−649.
29. Kalkum, M., Przybylski, M., and Glocker, M. O. (1998) Structure characterization of functional histidine residues and carbethoxylated derivatives in peptides and proteins by mass spectrometry, *Bioconjugate Chem. 9*, 226−235.
30. Tambe, D. R., Kuhn, A. M., Brossette, T., Giffhorn, F., and Scheidig, A. J. (2006) Crystal structure of NADP(H)-dependent 1,5-anhydro-D-fructose reductase from *Sinorhizobium morelense* at 2.2 Å resolution: construction of a NADH-accepting mutant and its application in rare sugar synthesis, *Biochemistry 45*, 10030−10042.

BI700281X